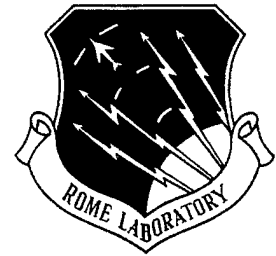


**RL-TR-97-200**  
**Final Technical Report**  
**October 1997**



# **OPTICAL WAVELET TRANSFORM**

**Florida Institute of Technology**

**Samuel P. Kozaitis**

*APPROVED FOR PUBLIC RELEASE; DISTRIBUTION UNLIMITED.*

19980310 165

**DTIC QUALITY INSPECTED 4**

**Rome Laboratory**  
**Air Force Materiel Command**  
**Rome, New York**

This report has been reviewed by the Rome Laboratory Public Affairs Office (PA) and is releasable to the National Technical Information Service (NTIS). At NTIS it will be releasable to the general public, including foreign nations.

RL-TR-97-200 has been reviewed and is approved for publication.

APPROVED:



MARK A. GETBEHEAD  
Project Engineer

FOR THE DIRECTOR:



DONALD E. HANSON, Director  
Surveillance & Photonics

If your address has changed or if you wish to be removed from the Rome Laboratory mailing list, or if the addressee is no longer employed by your organization, please notify RL/OCPA, 25 Electronic Pky, Rome, NY 13441-4515. This will assist us in maintaining a current mailing list.

Do not return copies of this report unless contractual obligations or notices on a specific document require that it be returned.

REPORT DOCUMENTATION PAGE			Form Approved OMB No. 0704-0188	
Public reporting burden for this collection of information is estimated to average 1 hour per response, including the time for reviewing instructions, searching existing data sources, gathering and maintaining the data needed, and completing and reviewing the collection of information. Send comments regarding this burden estimate or any other aspect of this collection of information, including suggestions for reducing this burden, to Washington Headquarters Services, Directorate for Information Operations and Reports, 1215 Jefferson Davis Highway, Suite 1204, Arlington, VA 22202-4302, and to the Office of Management and Budget, Paperwork Reduction Project (0704-0188), Washington, DC 20503.				
1. AGENCY USE ONLY (Leave blank)	2. REPORT DATE October 1997	3. REPORT TYPE AND DATES COVERED Final Jul 96 - Jul 97		
4. TITLE AND SUBTITLE OPTICAL WAVELET TRANSFORM		5. FUNDING NUMBERS C - F30602-96-2-0023 PE - 62702F PR - 4600 TA - P4 WU - PY		
6. AUTHOR(S) Samuel P. Kozaitis		8. PERFORMING ORGANIZATION REPORT NUMBER N/A		
7. PERFORMING ORGANIZATION NAME(S) AND ADDRESS(ES) Florida Institute of Technology 150 W. University Blvd Melbourne FL 32901-6988		10. SPONSORING/MONITORING AGENCY REPORT NUMBER RL-TR-97-200		
9. SPONSORING/MONITORING AGENCY NAME(S) AND ADDRESS(ES) Rome Laboratory/OCPA 25 Electronic Pky Rome NY 13441-4515		11. SUPPLEMENTARY NOTES Rome Laboratory Project Engineer: Mark A. Getbehead/OCPA/(315) 330-4146		
12a. DISTRIBUTION AVAILABILITY STATEMENT Approved for Public Release; Distribution Unlimited		12b. DISTRIBUTION CODE		
13. ABSTRACT (Maximum 200 words) We described a joint-transform correlator (JTC) that used multiple input images encoded in the spatial domain. This allowed various combinations of cross-correlations between input images to be performed. We extended the theory of a JTC to multiple inputs, and provided experimental results for four inputs with an optically-addressed spatial light modulator in the Fourier plane. We proposed a system to perform multiwavelet feature extraction. For m wavelet scales, the output consisted of 4m-1 correlation results, one of which is the desired result. Using conventional optics, the space-bandwidth product for wavelet feature extraction can be made the same as for a two-input joint-transform correlator.				
14. SUBJECT TERMS Pattern Recognition, Correlation, Optical Wavelet Transform		15. NUMBER OF PAGES 32		16. PRICE CODE
17. SECURITY CLASSIFICATION OF REPORT UNCLASSIFIED	18. SECURITY CLASSIFICATION OF THIS PAGE UNCLASSIFIED	19. SECURITY CLASSIFICATION OF ABSTRACT UNCLASSIFIED	20. LIMITATION OF ABSTRACT UL	

## 1.0 Introduction

The main difference between a joint-transform correlator (JTC) and a conventional Vanderlugt (4f) correlator is that the images in the JTC are encoded in the spatial domain. In terms of their output, both types of correlators perform the same operation, the cross-correlation between two images. In a 4f correlator, the Fourier transform of an input image is imaged onto the Fourier transform of a reference image. In a JTC, both input and reference images are input simultaneously in the spatial domain, then the Fourier transform is performed. The JTC has certain advantages when compared to the 4f correlator such as ease of alignment and avoiding spatial filter synthesis.<sup>1,2</sup>

Although most configurations of the JTC use two input images, the use of multiple input images may allow additional functions to be performed. For example, an image and two different wavelets were used in a JTC for multispectral (multiwavelet) wavelet feature extraction of the image.<sup>3</sup> In this approach, different versions of an input image corresponding to different wavelet scales appeared at different locations in the output plane. Another JTC configuration used three inputs, but required an additional electronic optical processing step to implement the wavelet transform.<sup>4</sup> In addition, another approach used two SLMs with a holographic mask to produce a wavelet-based JTC.<sup>5</sup> Although the wavelet transform has provided an application for a JTC with multiple inputs<sup>6</sup>, a generalized JTC with multiple inputs may find more applications including those in other areas if its output function was properly described.

We described a JTC that used multiple input images encoded in the spatial domain. In the next section we briefly described the general theory of a conventional JTC, and then extended the discussion to multiple inputs. Next, we provided some experimental results to verify the results of the theory. We also described how a multiple-input JTC can be used for multiwavelet analysis and proposed an architecture that has the same space-bandwidth product as a two-input JTC.

## 2.0 Conventional joint-transform correlator

To perform the correlation operation with a JTC, functions are encoded in the input plane.

A schematic diagram of a conventional JTC is shown in Fig. 1. To perform the cross-correlation between the images  $b(x,y)$  and  $d(x,y)$ , they are centered at  $x = \pm\alpha$ . A lens produces the Fourier transform when the input plane is illuminated with coherent light. In the Fourier plane, the complex light field is

$$U = B(p, q) e^{j\alpha p} + D(p, q) e^{-j\alpha p}, \quad (1)$$

where  $B(p,q)$  is the Fourier transform of  $b(x,y)$ , and similarly for  $d(x,y)$ . A square-law device such as a liquid crystal light valve is placed in the Fourier plane before an another lens performs the Fourier transform. Alternatively, a camera can be used to record the power spectrum and display it on a spatial light modulator (SLM) before the Fourier transform is performed. The output intensity distribution from a square-law detector can be written as

$$|U|^2 = UU^* = [B(p, q) e^{j\alpha p} + D(p, q) e^{-j\alpha p}] [B(p, q) e^{j\alpha p} + D(p, q) e^{-j\alpha p}]^*. \quad (2)$$

Multiplying terms, taking the Fourier transform, and grouping terms results in

$$I = b(x, y) \otimes b(x, y) + d(x, y) \otimes d(x, y) + b(x, y) \otimes d(x + 2\alpha, y) + d(x, y) \otimes b(x - 2\alpha, y), \quad (3)$$

in the output plane, where  $\otimes$  indicates the correlation operation. The first two terms are the auto-

correlations of the input functions and appear on the optical axis. The third and fourth terms are the cross-correlation between the two input functions and appear at  $x = \pm 2\alpha$  shown in Fig. 1.

### 3.0 Multiple-input joint transform correlator

We considered a JTC with an arbitrary number of input images arranged along a line. We used the JTC as in Fig. 1 but considered  $n$  inputs separated by  $\alpha$  in the input plane arranged along the  $x$ -axis as shown in Fig. 2. The images were labeled  $a_1(x,y)$  to  $a_n(x,y)$ , with the center image labeled as  $a_{(n+1)/2}(x,y)$ . Using this configuration, the complex light field in the Fourier plane was

$$U = A_1(p, q) e^{j\left(\frac{n-1}{2}\right)\alpha p} + A_2(p, q) e^{j\left(\frac{n-3}{2}\right)\alpha p} \dots \frac{A_{n+1}(p, q)}{2} + \dots A_n(p, q) e^{-j\left(\frac{n-1}{2}\right)\alpha p} \quad (4)$$

The output intensity distribution from a square-law detector was written as  $|U|^2 = U \times U^*$ . Multiplying  $n \times n$  terms, taking the Fourier transform, and grouping terms resulted in  $2n - 1$  locations in the output plane where a correlation response would occur. The output plane was described as

$$I = \left[ \sum_{i=1}^n a_i(x, y) \otimes a_i(x, y) \right] + \left[ \sum_{i=1}^{n-1} a_i(x, y) \otimes a_{i+1}(x + \alpha, y) + \sum_{i=1}^{n-2} a_i(x, y) \otimes a_{i+2}(x + 2\alpha, y) + \dots \sum_{i=1}^{n-(n-1)} a_i(x, y) \otimes a_{n-1}(x + (n-1)\alpha, y) \right] + \left[ \sum_{i=1}^{n-1} a_{i+1}(x, y) \otimes a_i(x - \alpha, y) + \sum_{i=1}^{n-2} a_{i+2}(x, y) \otimes a_i(x - 2\alpha, y) \right]$$

$$\dots \left[ \sum_{i=1}^{n-(n-1)} a_{n-1}(x, y) \otimes a_i(x-(n-1)\alpha, y) \right]. \quad (5)$$

The first term in brackets in Eq. (5) contains the DC terms which is the sum of the auto-correlations of all the input images. The second term in brackets correspond to  $n - 1$  terms to the left of the DC term which are shown in Fig. 3; each one of these terms is separated by a distance  $\alpha$ . The third term is similar to the second but corresponds to the right of the DC term in Fig. 3. In addition, the terms on each side of the DC term are the same but rotated by  $\pi$  radians as in a conventional JTC.

#### 4.0 Experimental results with the multiple-input JTC

We obtained experimental results to verify the operation of a multiple-input JTC. We used a JTC with an input displayed on film and an optically addressed SLM in the Fourier plane. We used a model SPT-25 optically-addressed SLM operating in a transmissive mode, manufactured by Micro-Optics Technologies Inc. To operate the device, light of 400nm - 500nm is used as write light which is absorbed by a photosensor layer. Light of 600nm - 1100nm is used as the read light that carries the write-light information. A DC bias of 2V - 15V is placed across the device for proper operation.

Our experimental set-up is shown schematically in Fig. 4. The Argon laser used a 10x microscope objective, 25 $\mu$ m pinhole and  $f = 250$  mm lens in the spatial filter assembly. The filter was a narrowband laser filter centered at 515 nm. Note that this wavelength is outside of the specification of the SLM, but we obtained better results with this line than with the 488nm line of the laser. The illuminating light just before the input plane had a power of 4.0 mW and both Fourier transform lenses had a focal length of  $f = 500$ mm. The He-Ne laser used as the read light of the SLM used a 10x microscope objective, 10 $\mu$ m pinhole and  $f = 250$  mm lens in the spatial filter assembly. The voltage across the SLM was 12.5V.

The input plane consisted of four of the same images as shown in Fig. 5 where  $\alpha = 1.5\text{mm}$ . The images were each labeled as  $f(x,y)$  and substituted into Eq. (5), and the expected output plane was described schematically as in Fig. 6. The output plane consisted of a bright spot on the optical axis and four responses on either side. The responses located at distances  $\alpha$  and  $3\alpha$  from the optical axis had the same intensity, as did the responses located at  $2\alpha$  and  $4\alpha$ . The responses at  $\alpha$  and  $3\alpha$  differed from those at  $2\alpha$  and  $4\alpha$  by a factor of two which would correspond to a factor of four if the power spectrum was detected.

The experimental result corresponding to the left half of Fig. 6 when Fig. 5 was used as an input is shown in Fig. 7a. The optical axis corresponding to the center of Fig. 6 is shown to the far right of Fig. 7a. Two bright spots along the x-axis corresponded to the autocorrelation responses located at distances  $\alpha$  and  $3\alpha$  from the optical axis. Two additional autocorrelations appeared at a distance of  $2\alpha$  and  $4\alpha$  from the optical axis. A profile plot along the x-axis through the autocorrelation peaks is shown in Fig. 7b where the peaks can be seen more clearly.

## 5.0 Multiwavelet feature extraction

### 5.1 Wavelet transform

The wavelet transform has shown to be useful in many areas including that of pattern recognition.<sup>7</sup> The wavelet transform can be thought of as a correlation between a wavelet and an input signal. The two-dimensional wavelet transform of an image  $f(x,y)$  can be written as

$$W(a,b) = \iint f(x,y) \Psi_{ab}^*(x,y) dx dy, \quad (6)$$

where  $\Psi_{ab}(x,y)$  is a set of wavelets that are dilated and shifted versions of a wavelet  $\Psi(x,y)$ , where



$$\Psi_{ab}^*(x, y) = \frac{1}{a} \Psi\left(\frac{x-b_x}{a}, \frac{x-b_y}{a}\right), \quad (7)$$

where  $a$  is a scale factor and  $b_x$  and  $b_y$  are translations in the  $x$  and  $y$  directions respectively. To examine an image at a particular scale or frequency band, the image is cross-correlated with a wavelet at a particular scale.

To display a version of an input image that corresponds to one wavelet scale using a JTC, one input is the image of interest and the other is the wavelet function.<sup>8</sup> The resulting image then appears at the output of the JTC. Because wavelets have zero mean, this may present a difficulty in the implementation. To remove the DC component from the wavelet function, it was experimentally shown that the input functions could be encoded in phase to eliminate the DC component.<sup>3</sup>

## 5.2 Simulation

Under certain conditions the input arrangement in Fig. 2 could produce a version of an input image corresponding to multiple wavelet scales. We considered an example that produced a version of an input image that corresponded to two wavelet scales. In other words, the output image corresponded to the sum of the cross-correlations of the input image and two different wavelets. To perform this type of operation we referred to Fig. 2 and set  $n = 5$ , and  $a_3(x,y) = 0$ . We considered the input image  $f(x,y)$  at locations  $a_1(x,y)$  and  $a_2(x,y)$ , so  $f(x,y) = a_1(x,y) = a_2(x,y)$ . Finally, we set a wavelet corresponding to one scale  $w_1(x,y) = a_4(x,y)$ , and the wavelet at another scale  $w_2(x,y) = a_5(x,y)$  as shown in Fig. 8.

The response in the output plane was obtained by substituting the appropriate variables in Eq. (5), and was represented schematically as shown in Fig. 9. The third term from the DC is the term of interest here. It was the coherent sum of correlations of the input image and two different wavelets at two different scales. To simulate the result we used a Bessel-Gaussian wavelet.<sup>3</sup> The

Bessel-Gaussian wavelet was described as

$$\frac{1}{\sqrt{a}}w\left(\frac{r}{a}\right) = \frac{1}{\sqrt{a}}J_0\left(\frac{r}{a}\right)\exp\left[-\left(\frac{r}{2a\sigma}\right)^2\right] \quad (8)$$

where  $\sigma$  is related to the width of the bandpass response,  $a$  is the scale factor, and  $r$  is the distance from the origin.

We performed simulations with an image of an airplane  $f(x,y)$  shown in Fig. 10 placed into the configuration of Fig. 8 using a total of 512 x 512 pixels. The image of the plane contained 50 x 50 pixels and  $\alpha$  was set to 50 pixels. The Bessel-Gaussian wavelet was used for  $w_1(x,y)$  with  $a_1 = 0.7$  and  $w_2(x,y)$  with  $a_2 = 1.2$ . The output plane was shown in Fig. 11 and consisted of nine responses. The three responses consisting of the one along the optical axis, and the ones immediately to the right and left of the optical axis at  $\pm\alpha$  were autocorrelation responses. They all had large values and overlapped with each other. In addition, they overlapped the responses located  $\pm 2\alpha$  from the optical axis. Therefore, the large spot in Fig. 11 consisted of five correlation responses. This left four responses, two on each side of the large central spot. The two remaining responses on the left hand side of Fig. 11 were expanded and shown in Fig. 12a. The response on the left corresponded to the wavelet with  $a_2 = 1.2$  and the one on the right corresponded to the sum of the wavelets with  $a_1$  and  $a_2$ . Changing  $a_1$  to  $a_1 = 1.0$  changed the response on the right but not on the left as shown in Fig. 12b. A small part of the correlation between the image and the wavelet with associated with  $a_1$  can be seen in the left side of the image.

### 5.3 Implementation

To implement the multiple-input JTC optically a few points must be considered. One is the removal of the DC from the wavelet image. Wavelets have zero mean, so the wavelet image cannot be used directly. One solution is to display the wavelet in phase;<sup>3</sup> however, we proposed to use a DC block arrangement.

Because more than one scale of a wavelet is used in our arrangement, multiple wavelet images are needed; one for each scale of the wavelet used. Displaying multiple images on an SLM would increase the space-bandwidth product of the system, so we proposed to use conventional optics to produce different versions of the wavelet at different scales. Similarly for copying the input image.

A proposed multiple-input JTC configuration for the multiwavelet example was shown in Fig. 13. It used an input SLM to display an input image and wavelet image as in a conventional JTC. The DC of the wavelet could be eliminated using a DC block in the Fourier transform plane of a telescope arrangement. The scale of a wavelet could be adjusted by varying the focal length of lenses in another telescope arrangement. Neutral density filters may be used to adjust the amplitude of the wavelet. The input lens in the JTC must capture all images, but a detector is required for only a portion of the output plane.

## 6.0 Conclusion

We showed how a JTC can be used with multiple input images, and how a multiple-input JTC can be used for multiwavelet analysis of an input image. Using an image and wavelet as inputs, for  $m$  wavelet scales,  $m$  versions of the wavelet and  $m$  copies of the input image could be generated using conventional optics. The output consisted of  $4m-1$  correlation results, one of which is the desired output. Using conventional optics, the space-bandwidth product of the system can be made the same as for a two-input joint-transform correlator.

Because an output image can be produced that corresponds to multiple wavelet scales, the system is potentially more useful than one that corresponds to a single scale. In our demonstration the relationship between the wavelet scales was fixed. The relationship between the wavelet scales can be made independent by increasing the space-bandwidth of the system.

## 7.0 References

- [1] C. S. Weaver, and J. W. Goodman, "A technique for optically convolving two functions," *Appl. Opt.* **5**, 1248-1249 (1966)
- [2] *Real-time optical information processing*, B. Javidi, and J. L. Horner, Eds., Academic Press: San Diego, CA (1994)
- [3] P. S. Erbach, D. A. Gregory, and X. Yang, "Optical wavelet transform by the phase-only joint-transform correlator," *Appl. Opt.* vol. **35**(17), 3117-3126 (1996)
- [4] X. Yang, N. P. Cavaris, and M. Wen, "Optical wavelet correlators for cluttered target identification," in *Optical Pattern Recognition V*, SPIE 2237, 402-418 (1994)
- [5] J. Li, Y. Zhang, J. Hu, "Object recognition with a wavelet-transform-based joint transform correlator," *Opt. Eng.* vol. **35**(3), 775-777 (1996)
- [6] S. P. Kozaitis, M. A. Getbehead, and W. E. Foor, "Multispectral image feature extraction by the joint wavelet-transform correlator," in *Optical Pattern Recognition VIII*, D. P. Casasent, Ed., Proc. SPIE 3073, paper 34 (1997)
- [7] M. B. Ruskai, B. Beylkin, R. Coifman, I. Daubechies, S. Mallat, Y. Meyer, and L. Raphael, *Wavelets and Their Applications*, Jones & Bartlett: Boston, MA, (1992)
- [8] W. Wang, G. Jin, Y. Yan, and M. Wu, "Joint wavelet-transform correlator for image feature extraction," *Appl. Opt.* vol. **34**(2), 370-376 (1995)

up

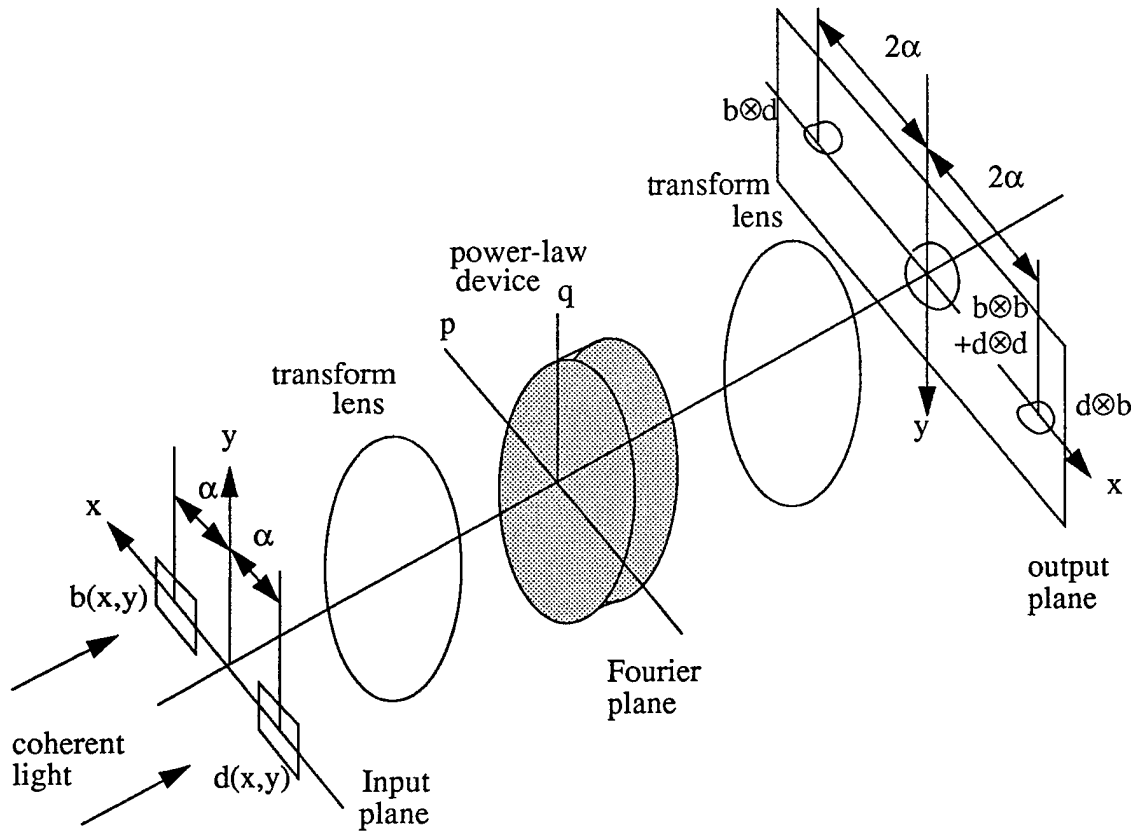


FIGURE 1. Schematic diagram of a conventional joint-transform correlator

up

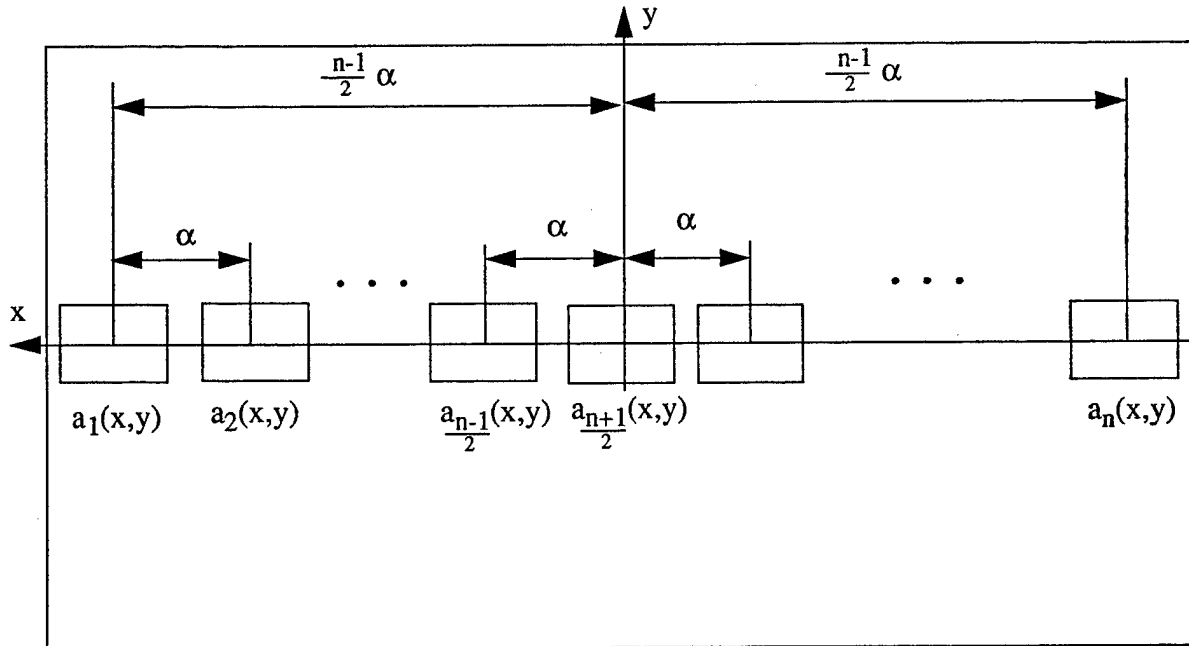


FIGURE 2. Input plane of multiple-input JTC

up

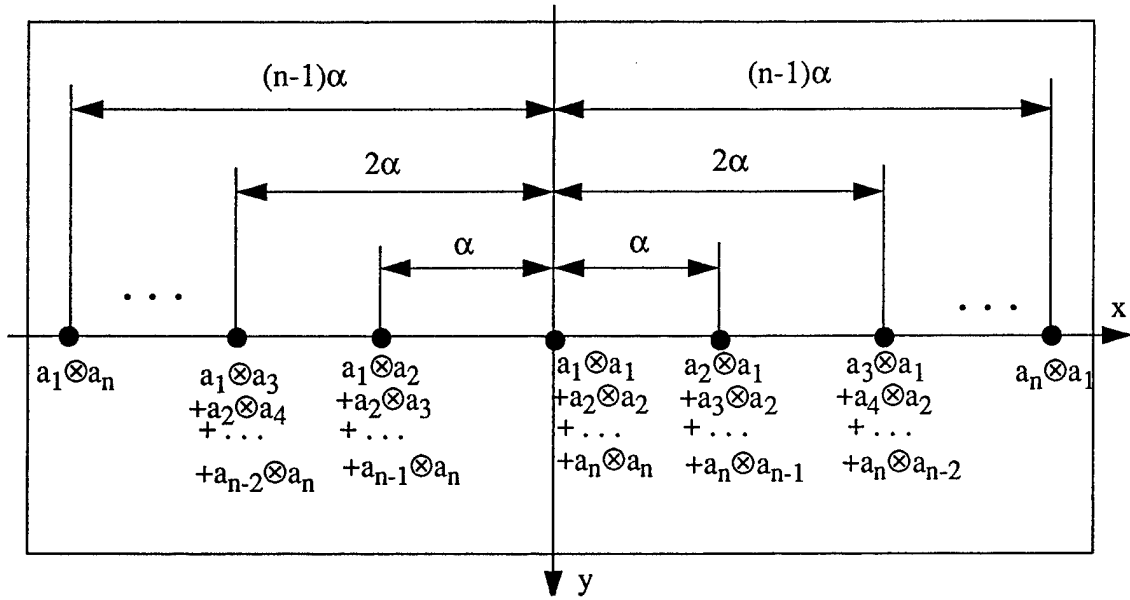


FIGURE 3. Output plane of multiple-input JTC

up

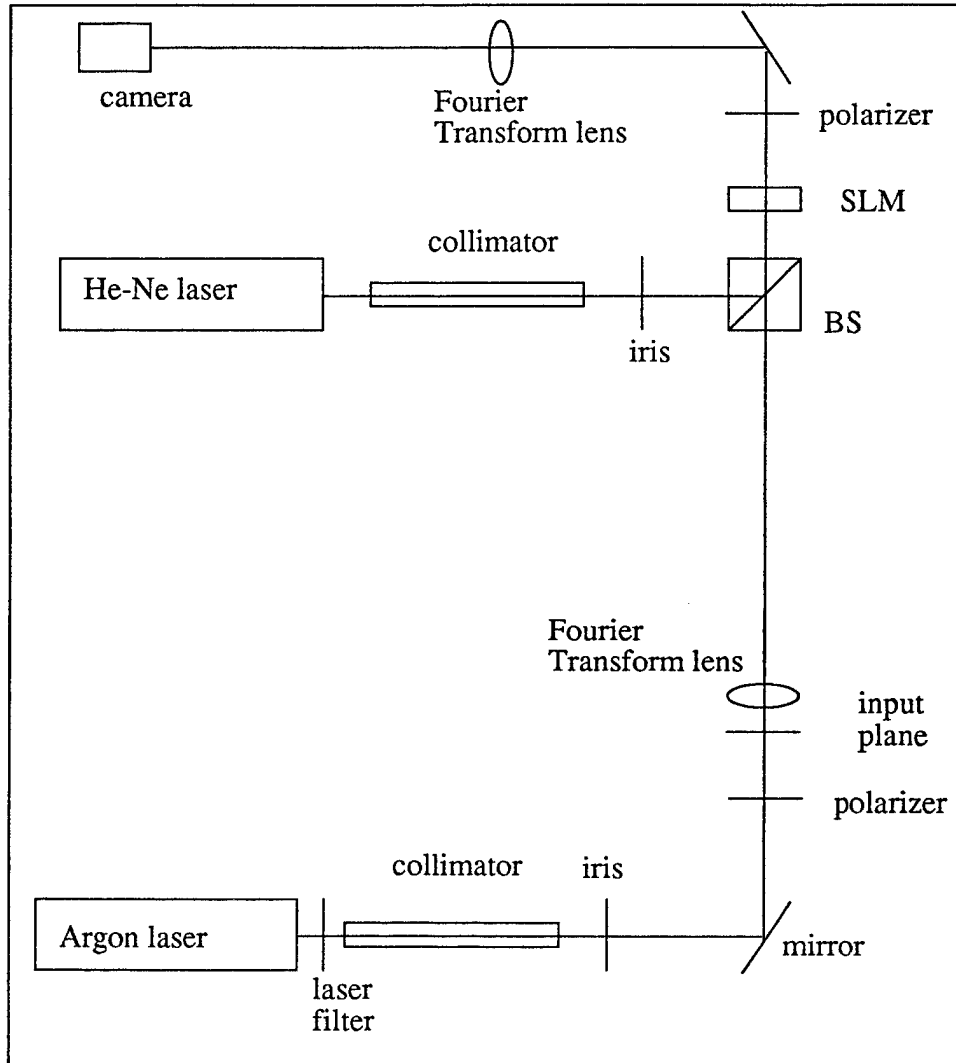
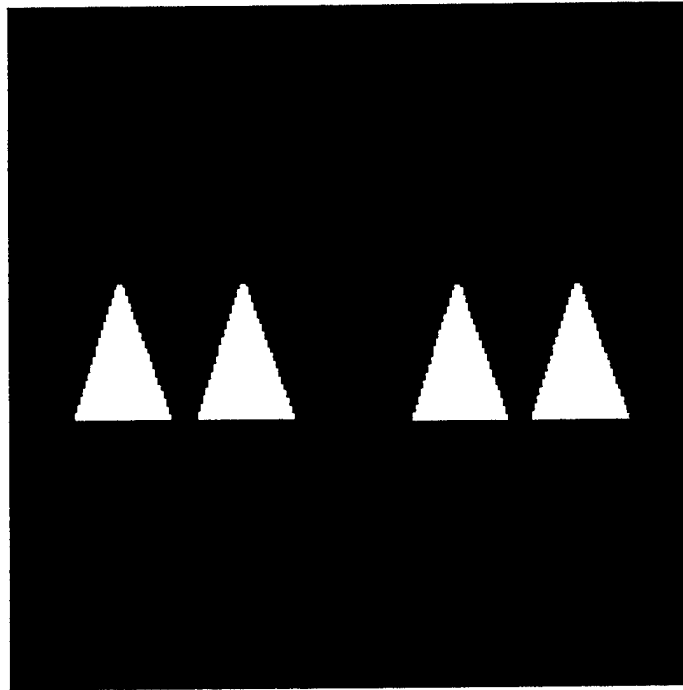


FIGURE 4. Experimental set-up of multiple input JTC



up



**FIGURE 5. Input image used in experiment**

up

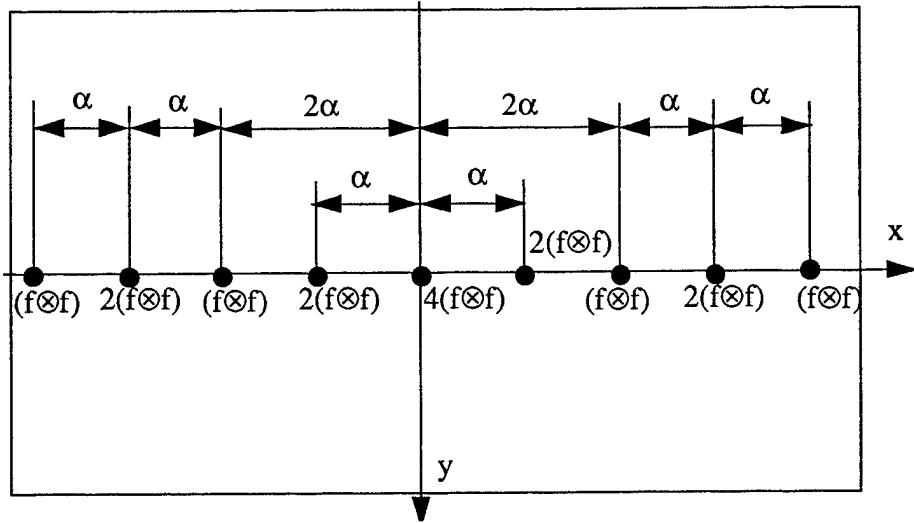
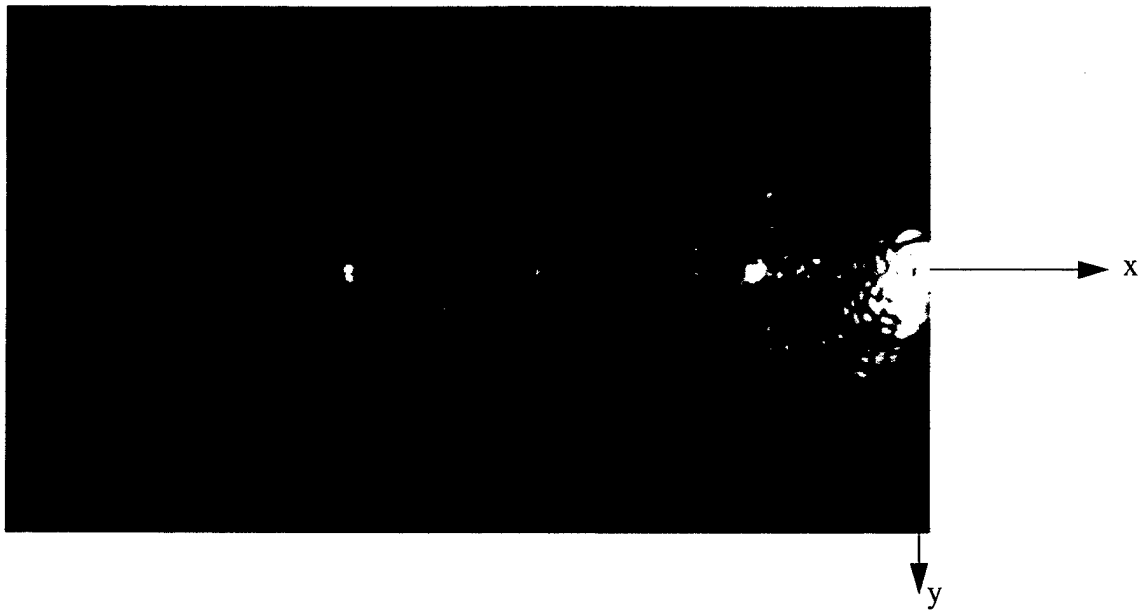
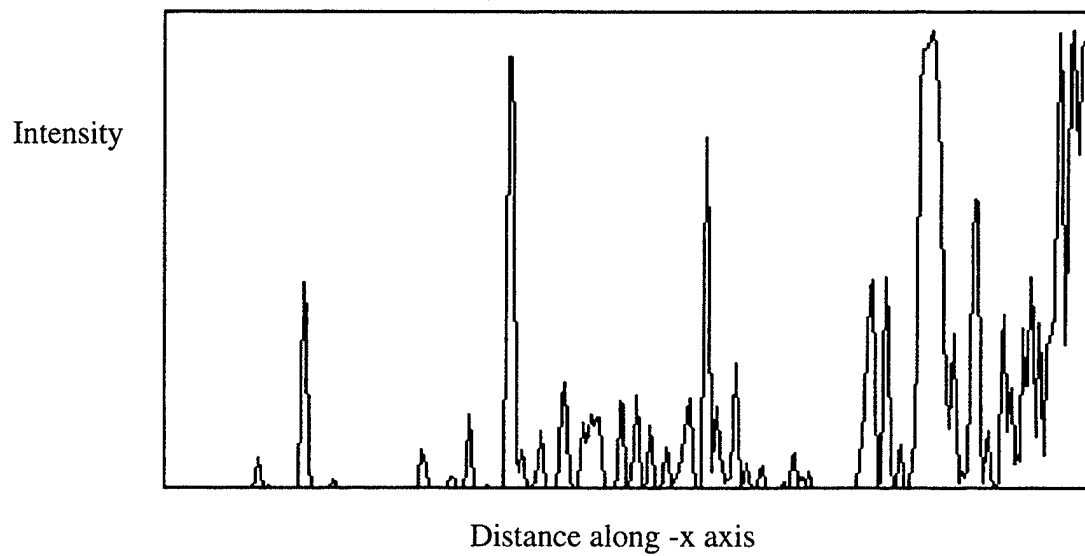


**FIGURE 6.** Location and relative value of correlation response of multiple-input JTC when Fig. 5 was used as the input.

up



(a)



(b)

**FIGURE 7. Left hand side of output plane obtained experimentally when Fig. 5 was used as the input plane.**

up

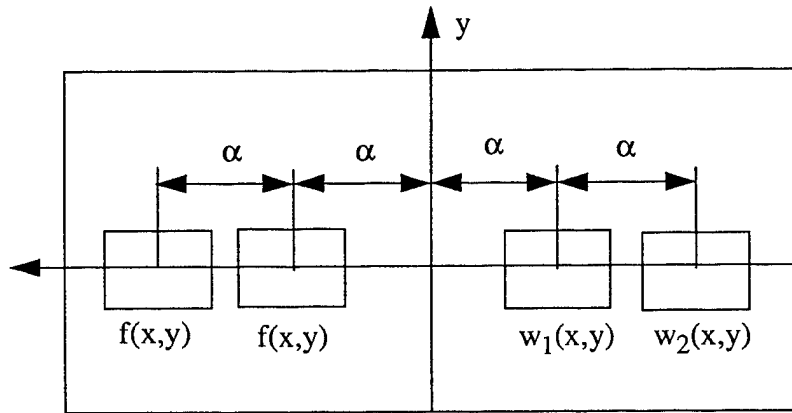


**FIGURE 8. Input plane of multiwavelet example**

up

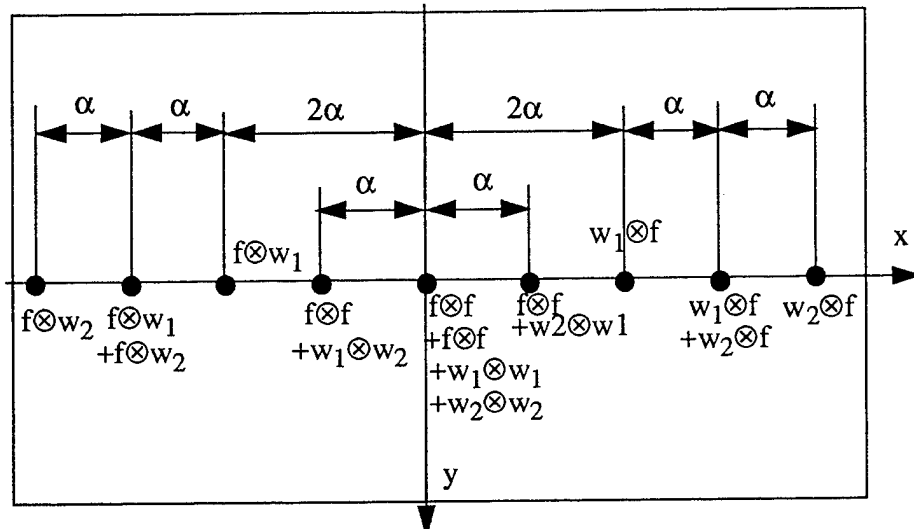
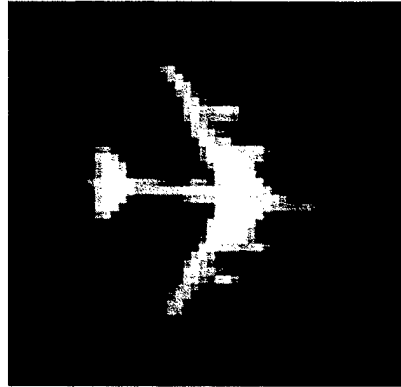


FIGURE 9. Output plane of multiwavelet example

up



**FIGURE 10. Image used in simulation experiments.**

up

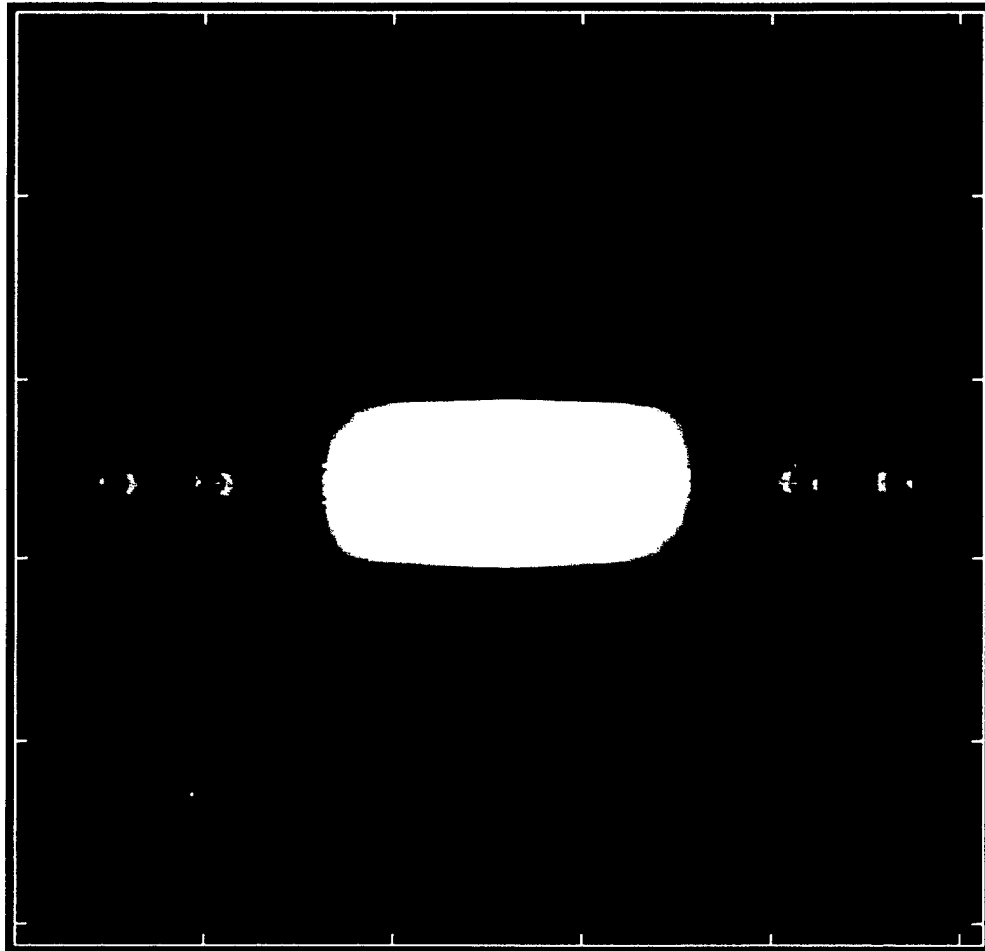
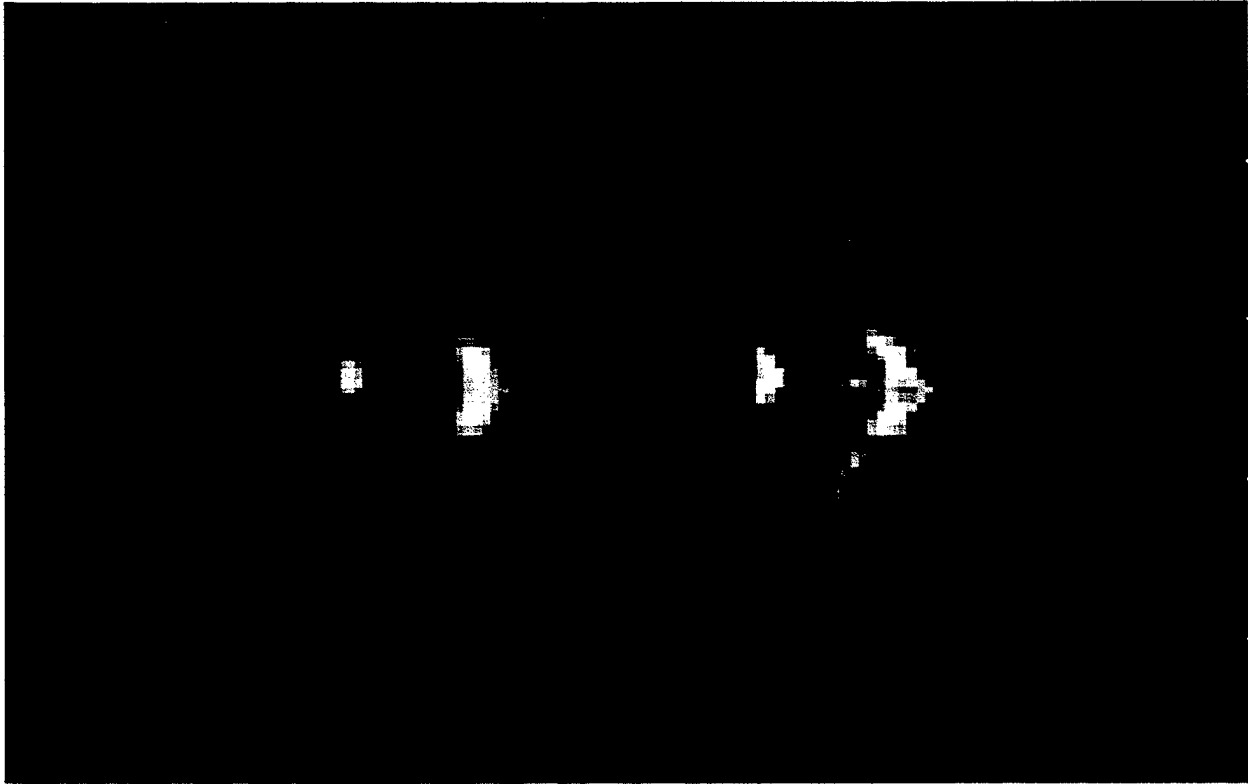


**FIGURE 11. Output plane of multiwavelet simulation experiment.**

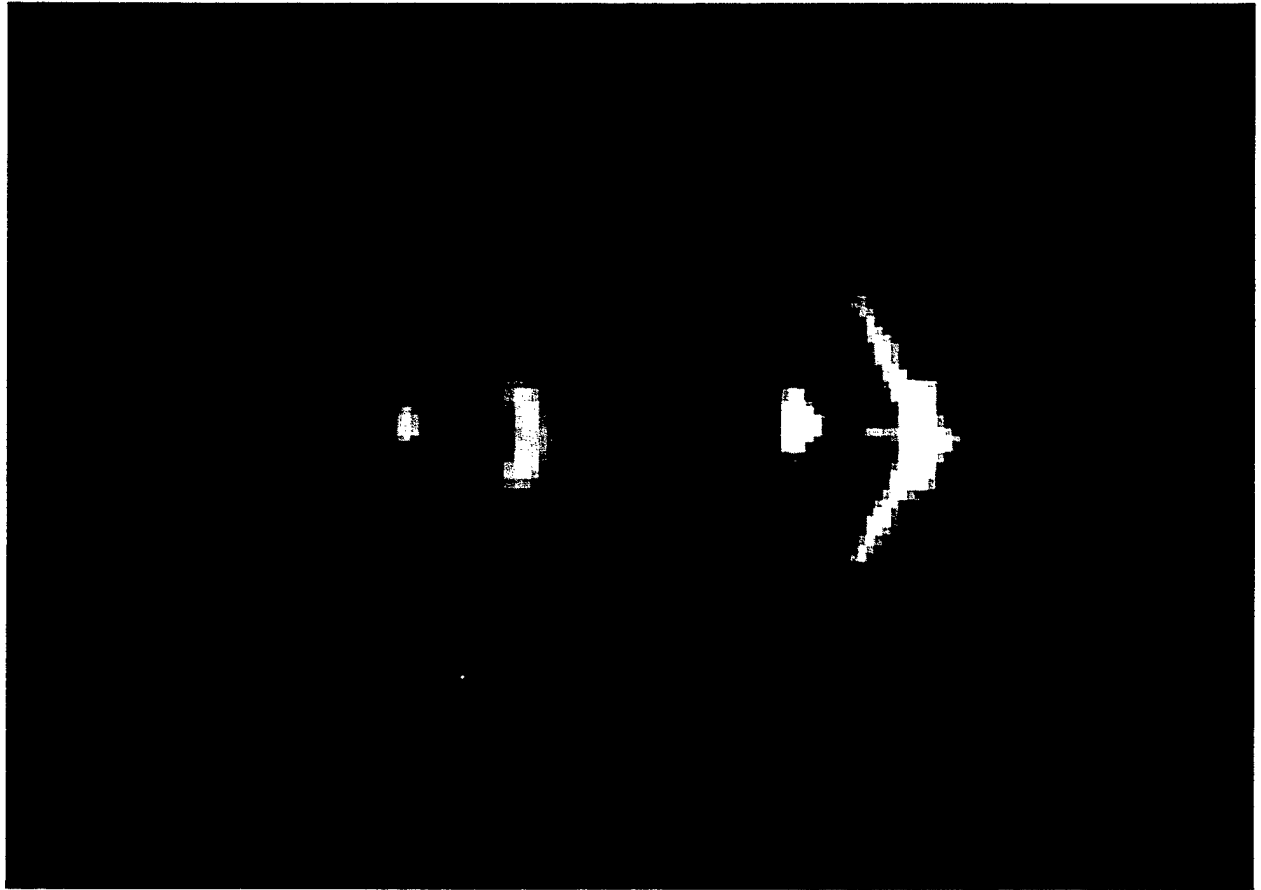
up



(a)



up



(b)

**FIGURE 12. Close-up view of left hand side of Fig. 11. Response on left in both cases is for  $a_2=1.2$ , (a) response of right is for  $a_1 + a_2$ , where  $a_1 = 0.7$  (b) response of right is for  $a_1 + a_2$ , where  $a_1 = 1.0$ .**

up

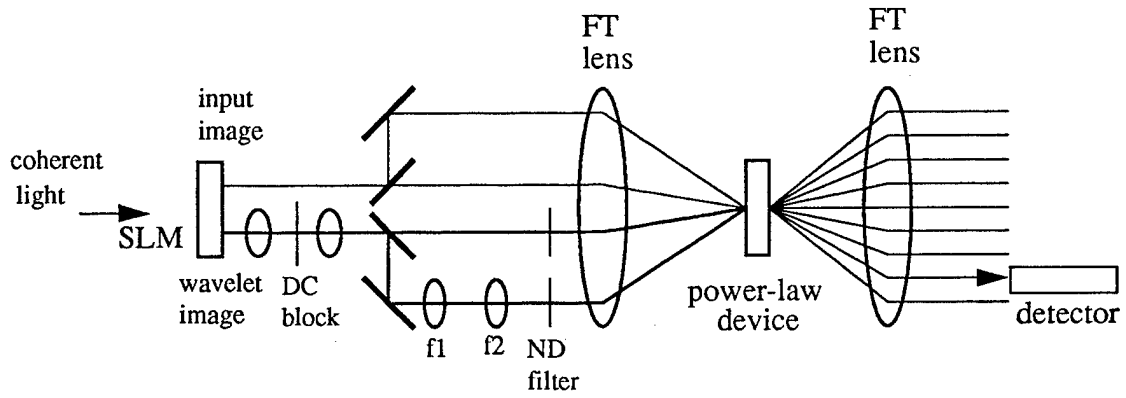


**FIGURE 13. Schematic diagram of multiple-input JTC used for multiwavelet analysis using two wavelet scales**

***MISSION  
OF  
ROME LABORATORY***

Mission. The mission of Rome Laboratory is to advance the science and technologies of command, control, communications and intelligence and to transition them into systems to meet customer needs. To achieve this, Rome Lab:

- a. Conducts vigorous research, development and test programs in all applicable technologies;
- b. Transitions technology to current and future systems to improve operational capability, readiness, and supportability;
- c. Provides a full range of technical support to Air Force Material Command product centers and other Air Force organizations;
- d. Promotes transfer of technology to the private sector;
- e. Maintains leading edge technological expertise in the areas of surveillance, communications, command and control, intelligence, reliability science, electro-magnetic technology, photonics, signal processing, and computational science.

The thrust areas of technical competence include: Surveillance, Communications, Command and Control, Intelligence, Signal Processing, Computer Science and Technology, Electromagnetic Technology, Photonics and Reliability Sciences.